Multiple Image SAR Shape-from-Shading

J. Thomas, W. Kober, and *F. Leberl*
VEXCEL Corporation, 2477 55th Street, Boulder, CO 80301

ABSTRACT: We describe a technique for combining radar image shape-from-shading with stereo radargrammetry to produce terrain surface models using multiple SAR images. This technique is expected to be of use to reconstruct surface shape from Magellan images of planet Venus, and to refine the results of terrestrial radar measurements.

Local variation in pixel shading is an indicator of terrain slope changes. This variation in pixel shading offers an opportunity for increasing the detail of terrain mapping over that which is available from stereo radargrammetry alone. Shape-from-shading can potentially provide a relative change in height at each pixel. This leads to a dense set of height measurements and a more faithful rendition of the local terrain shapes. However, shape-from-shading needs some type of boundary values or external terrain low-frequency information to succeed. These can be obtained from stereo or from altimeter measurements.

RADARGRAMMETRIC SURFACE RECONSTRUCTION

IMAGES CONTAIN local variation of pixel gray values which are related to changes in local relief as well as to changes in local thematic values. The process of extracting local slope information from the local shading variation is known as "shape-from-shading." Because the knowledge of terrain slopes can be used to infer terrain heights, shape-from-shading offers an approach for determining terrain heights. Because each pixel offers an independent measurement of slope, the technique is inherently pixel-based.

There are a variety of techniques available for terrain reconstruction using radar, including stereo, interferometry, altimetry, etc. Of these, stereoscopy is the most developed surface reconstruction technique (Leberl, 1976) and can be called the "classical method" for height determination from optical imagery. Stereoscopy uses the geometric disparity, or "parallax," for corresponding points in two or more images overlapping a common scene. The parallax is converted to a measurement of terrain height. The ability to estimate such heights usually depends on the sensor configuration used to obtain overlapping images, the image resolution, and the stability of the imaging process. As the resolution degrades, measurements of parallax become less precise (in object dimensions) until the range of height values disappears in the noise of parallax measurements.

Stereoscopic processing of synthetic aperture radar (SAR) offers additional constraints beyond those that apply to optical images. These relate to the fact that illumination of the terrain changes from flight line to flight line so that the ability to measure heights depends on the imaged surface as well. Therefore, image matching is perturbed by dissimilar illumination in overlapping images, as discussed by Ramapriyan *et al.* (1986) and Thomas *et al.* (1987). In order to reduce this effect, one uses radar image pairs with small distances between flight lines. This in turn has the effect that, even if SAR-parallax can be measured acurately, detailed terrain heights will not be resolved at the resolution of radar imagery. This limited height resolution results from poor error propagation and stereo intersection geometry, as described by Leberl (1976). In addition, of course, human operators and/or automated stereo algorithms rely on matching image regions. Consequently, even if match points were determined for every pixel, these match points are not independent samples of the parallax function, but are samples of the match function that relates regions in the two images. As a result, stereo measurements, by design, undersample the true terrain height (Figure 1). The terrain model reconstructed using stereo methods will of necessity be of lower resolution than is available from pixel-based methods such as shape-from-shading.

As we will discuss later, shape-from-shading also has significant limitations. However, one may argue that an ideal radar-image-based surface reconstruction system combines several techniques. Stereo techniques certainly produce direct height measurements, with reference to a global coordinate system centered at the sensor. This technique has been demonstrated operationally (Mercer *et al.*, 1989) using aircraft SAR. In contrast, shape-from-shading produces slope measurements, or local height differences, which require boundary values to produce actual heights. There is thus value in each type of measurement. Therefore, the challenge is to develop a methodology which integrates the measurements from these technologies to produce a more accurate and detailed description of the terrain than any one technique could provide alone. This study focuses on the combination of shape-from-shading with other techniques for measuring heights, in particular with stereo.

PRINCIPLES OF SHAPE-FROM-SHADING

Shape-from-shading requires the formulation of the reflectance map, R, which is an analytical description of the observed image $I(x,y)$ in terms of the surface coordinates x,y,z, image sensing vectors, and normalized scattering cross-section. We assume that the following parameters are the determinants of a reflectance map, R, as stated by Frankot and Chellappa (1987a):

$$I(x,y) = R(z_x, z_y, \beta, L, \sigma_0) \tag{1}$$

where $z(x,y)$ = an expression for terrain height,
z_x, z_y = slopes in x and y direction,
β = illumination vector,
L = boresight vector, and
σ_0 = albedo.

Equation 1 is valid for a variety of sensors, including the imaging radar. Note that "albedo," the generic term for reflective surface properties, is represented in the radar case by the scattering cross section σ_0.

The image gray values $I(x,y)$ are then the discretized levels between the minimum and maximum radiometric values. $I(x,y)$ is observed through a radar image; the terrain slopes z_x, z_y, and the local normal $\hat{\mathbf{n}}$, a vector, are related by Equation 2 and are to be estimated: i.e.,

$$\hat{\mathbf{n}} = (z_x, z_y, (1 - z_x^2 - z_y^2)^{1/2}) \tag{2}$$

An exact functional relationship among the variables $(z_x, z_y, \beta, L, \sigma_0)$, is intractable to derive analytically, and in the past has been the subject of empirical studies and some simplified modeling of the scattering mechanisms involved. Difficulties arise from the complicated response of surface shape and terrain cover to radar.

PHOTOGRAMMETRIC ENGINEERING & REMOTE SENSING,
Vol. 57, No. 1, January 1991, pp. 51–59.

0099-1112/91/5701–51$03.00/0

FIG. 1. Segment of a radar image map. Radar stereo derived contours superimposed over an image. Solid contour lines have a 100-m interval. Area covered is 5km by 4km. Note that contour lines do not model to smaller topographic relief elements, characterizing the coarseness of the stereo-based elevation. (Area: Brazeau Range, Alberta, Canada. Imagery: Intera Technologies Ltd., STAR-2, 6-m resolution, X-Band).

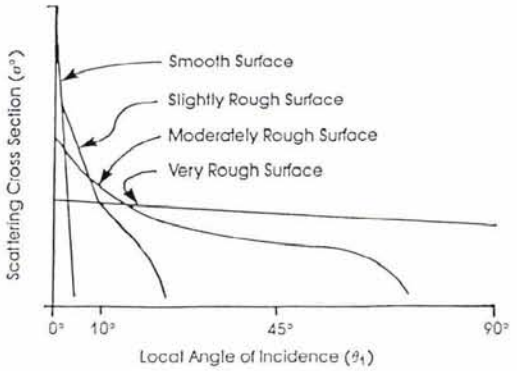

FIG. 2. Plots of normalized scattering cross sections (also denoted as radar backscatter coefficients) versus local incidence angle. This shows that surface properties change as the angle at which radiation hits the surface varies. The type of change is a function of roughness and electrical properties of the material (from Kaupp *et al.*, 1981).

In most radar shape-from-shading studies, a number of simplifying assumptions have been made. An example is the study presented by Wildey (1986a) in which the reflectance map was assumed to follow the cosine law. In such a formulation the image brightness is modeled as the cosine of the angle between the illumination vector and the local normal. The cosine model assumes that the normalized scattering cross section coefficient, σ_0 does itself not vary with local incidence angle. Figure 2 illustrates that this assumption is a gross simplification. However, this reflectance model was used in our study to develop an initial understanding of the basic issues of radar shape-from-shading. More complex models of the reflectance map will be used in future efforts.

Single image shape-from-shading cannot resolve the fundamental ambiguity between changes in albedo and slope when a change in shading is encountered. Even with the assumption of uniform albedo, the problem of height reconstruction from shading is mathematically underdetermined. The shading information from single pixels merely implies a cone constraint of the local surface normal (Figure 3) as stated by Wildey (1986a).

The single image algorithm derived by Frankot and Chellappa (1987a) was posed as a calculus of variations problem and involved minimizing the following cost function.

$$\epsilon = \iint (I(x,y) - R(z_x,z_y))^2 + \lambda(z_{xx}^2 + 2z_{xy}^2 + z_{yy}^2)\, dxdy \quad (3)$$

where

I = actual image gray value,
R = reflectance map,
z_x = slope in the range direction,
z_y = slope in the azimuth direction,
z_{xx} = second partial derivative of z in the range direction,
z_{xy} = partial derivative of z with respect to x,y directions,
z_{yy} = second partial derivative of z in the y direction, and
λ = regularization parameter.

The first term in Equation 3, $(I(x,y) - R(z_x,z_y))^2$, is a measure of the difference between the pixel gray values of an actual image versus the values predicted using the current estimated terrain model. Because of the mathematically ill-posed nature of such inverse problems (Baltes, 1980), solutions which minimize this term will lead to very oscillatory terrain estimates.

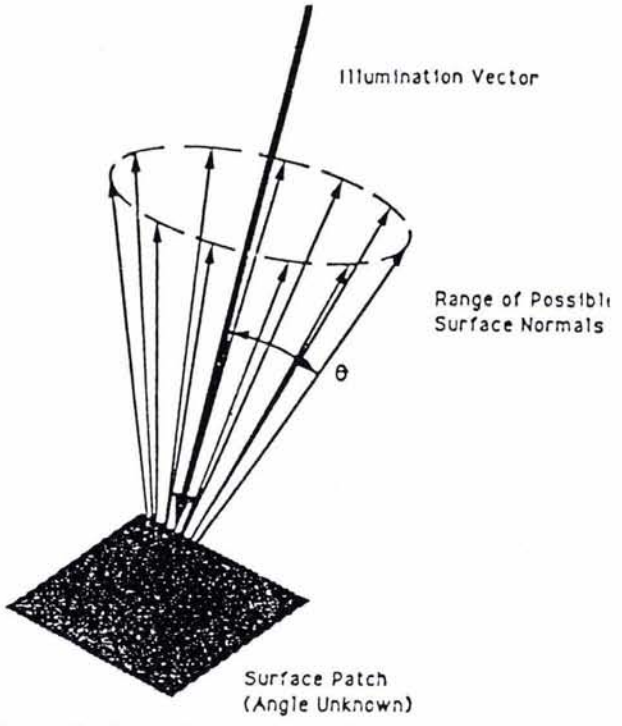

FIG. 3. Shading implies a cone constraint on surface normals: a specific image pixel gray value, with assumed electrical properties of the corresponding surface patch, only defines an infinite range of possible surface normals.

Therefore, a regularization term, $\lambda(z_{xx}^2 + 2z_{xy}^2 + z_{yy}^2)$, is included to act as a penalty function that limits the amount of terrain oscillations. In this way, solutions to the combined metric represent a comprise between faithful image prediction and terrain slope variations.

The reconstruction problem is thus formulated as a calculus of variations problem, the solution to which is obtained using the Euler-Lagrange equations (Marion, 1965). The form of the solution, thus obtained, is one in which the estimates of the terrain slopes are iteratively improved. The slopes are then integrated to calculate heights.

One very useful condition for integrating slopes involves the notion of "integrability." Analytically, this condition implies that

$$z_{xy}(x,y) = z_{yx}(x,y) \tag{4}$$

where $z(x,y)$ is the analytical expression for the terrain surface.

Using Strokes' theorem, as described by Schey (1973), it is trivial to show that the requirement in Equation 4 ensures that the integral of the slopes over any closed path reduces to zero. In practice, then, requiring the condition in Equation 4 ensures that the slopes can be integrated along any path to calculate heights.

Most earlier approaches to shape-from-shading produced height models that did not satisfy integrability. Horn and Brooks (1986) used a penalty function to drive the interrated solution toward integrable solutions. In practice, this meant that the computed solution usually was only "close" to being integrable. A more rigorous effort was presented by Frankot and Chellappa (1987b) wherein the latest estimated solution was projected onto an integrable subspace of solutions on every iteration to calculate heights. This projection is accomplished in the Fourier domain and is given by

$$C(\omega = \frac{C_1(\omega)P_x(\omega) + C_2(\omega)P_y(\omega)}{|P_x(\omega)|^2 + |P_y(\omega)|^2} \tag{5}$$

where

- $C(\omega)$: is the Fourier transform of the integrable height model,
- $C_1(\omega)$: is the Fourier transform of the estimated slopes in the x-direction,
- $C_2(\omega)$: is the Fourier transform of the estimated slopes in the y-direction,
- ω: is the Foureir domain frequency variable, and
- $P(\omega)$: is the Fourier coefficients of a discrete differentiation operator in x and y.

Most early work on shape-from-shading dealt with optical imagery, as summarized by Horn and Brooks (1989), and including work reported by Shao *et al.* (1988). Specific radar-based studies include works reported by Frankot and Chellappa (1987a, 1987b), Guindon (1989), Kirk (1987), and Wildey (1986a, 1986b, 1987, 1988a, 1988b). All of the techniques reported above only deal with single images. Several different approaches for reconstructing the surface shapes from multiple images have been derived and is discussed by Thomas *et al.* (1989). In the following we discuss the implèmentation and results obtained using one of these methods which we will call the generalized cost function approach. This generalized formulation is obtained by generalizing the single image formulation by Frankot and Chellappa (1987a).

GENERALIZED COST FUNCTION APPROACH FOR MULTIPLE IMAGES

A generalization of the algorithm in Equation 3 to N images involves minimizing the following cost function (superscripts refer to image number):

$$\epsilon = \iint \lambda_1(I^{(1)}(x,y) - R^{(1)}(z_x,z_y))^2 + \lambda_2 (I^{(2)}(x,y) - R^{(2)}(z_x,z_y))^2 + \ldots + \lambda_N(I^{(N)}(x,y) - R^{(N)}(z_x,z_y))^2 + \lambda(z_{xx}^2 + 2z_{xy}^2 + z_{yy}^2)\, dxdy \tag{6}$$

Upon minimizing the N-image cost function, we have (Thomas *et al.*, 1989a):

$$\begin{bmatrix} z_x \\ z_y \end{bmatrix} = \begin{bmatrix} \overline{z_x} \\ \overline{z_x} \end{bmatrix} + \frac{3\epsilon^2}{10\lambda}\left(\lambda_1(I^{(1)} - R^{(1)}) \begin{bmatrix} R_{z_x}^{(1)} \\ R_{z_y}^{(1)} \end{bmatrix} + \ldots + \lambda_N(I^{(N)} - R^{(N)}) \begin{bmatrix} R_{z_x}^{(N)} \\ R_{z_y}^{(N)} \end{bmatrix}\right) \tag{7}$$

where $\overline{z_x}$ is a local average defined by $\overline{a_{i,j}} = 1/4[a_{i,j+1} + a_{i+1,j} + a_{i,j-1} + a_{i-1,j}]$ where i,j refer to indices in the data array, and a is the variable averaged.

In the generalization presented above, it is assumed that the reconstructed terrain model and all images are in the same coordinate system. This assumption is satisfied by the first using radar stereo matching to acquire an approximate height model and using this height model to ortho-rectify (geocode) the iamges.

At each iteration, the latest slope estimates derived from Equation 6 are convereted to a height model using the Fourier projection technique given by Equation 5. In this technique, non-integrable slopes, z_x,z_y are Fourier transformed and projected onto an integrable surface so that the resulting height model and thus the slopes are integrable (i.e., they satisfy Equation 4).

BOUNDARY CONDITIONS

Another modification of the single-image algorithm is the correction of estimated heights in the Fourier projection step described above, to take into account *a priori* knowledge of some spot heights obtained from stereoscopy or altimetry. Such spot height values represent constraints on the estimated height values. These constraints can be reinforced at each iteration as a correction to the heights obtained following the Fourier projection step to obtain heights from slopes.

However, reinforecement at each iteration of a "hard" constraint, such as these spot heights, tends to cause an oscillatory "ringing" in the estimated surface. Therefore, such corrections are made in a "soft" mode. This means that corrections are made using a given fraction of the difference between the constraint value and the estimated value at each iteration. As the iteration number increases, the fraction of the difference between the constraint value and the estimated value can be allowed to increase.

The use of a soft version of a constraint rather than a "hard" constraint is generally useful in iterative optimization problems, because there may be no connected path from a suboptimal solution to the optimal solution which satisfies the hard constraint. However, by continuity, a path exists consisting of suboptimal solutions which satisfy soft constraints.

Another approach is to analytically incorporate spot heights into the reconstruction process as estimates of the terrain low frequencies. In this way both *a priori* height and slope information contribute to the integradable height model obtained. The mathematical issues concerning this approach are treated by Thomas *et al.* (1989a).

The low frequency enforcement method fits naturally into the Fourier domain implementation of the integration process. Unlike the spot height enforcement method, which showed a lack of robustness, even when a "soft" version was used, the low frequency enforcement method was very well behaved and more effective (i.e., the process converged in far fewer iterations).

Another constraint on the reconstructed model is the ranges measured by the radar, i.e, the constructed height model must satisfy the radar range equations given the location of the radar with respect to the height model. Note that, for multiple images, this constraint reduces to the stereo condition. The range constraint algorithm has been mathematically formulated as described by Thomas *et al.* (1989a) and is currently being investigated for implementation.

IMPLEMENTATION AND PROCESSING

For an analysis of shape-from-shading, the algorithm described earlier was implemented. Numerous experients were conducted with a variety of test images taken by an aircraft SAR. The height reconstruction process consists of the following sequence of steps:

(1) The aircraft SAR images are processed using stereo techniques to derive a (preliminary) height model and to rectify the images using this height model.
(2) These approximately rectified images have a pixel size of 6m and are averaged down to 24-m pixels to reduce effects of speckle.
(3) The rectified image and the stereo derived height models are used as input into the shape-from-shading program. The shape-from-shading process includes up-dating the slope estimates using Equation 6, simultaneously projecting the slopes onto an integrable surface and integrating to derive heights using Equation 5, and recomputing slopes to be used again in Equation 6. In the integration process, the low frequency components of the current estimate of the height model are constrained to remain consistent with the low frequencies of the stereo derived height model.

Because the shape-from-shading process is iterative, its convergence is monitored by evaluating the cost function (Equation 5) at every iteration. The process was stopped when the change in the cost from one iteration to the next was sufficiently small. For the results presented in the following, the number of iterations required was about 40.

RESULTS AND DISCUSSION

An analytical study of the shape-from-shading algorithm was performed and wil be reported separately. In the following we discuss some experimental results.

Initial tests of shape-from-shading focused on using simulated radar images. The results with both single image and multiple image versions were presented by Thomas *et al.* (1989b). Current results were obtained using actual radar images. The processed data consist of subwindows of 128 by 128 pixels averaged down to 24m from 6m. Therefore, all presentations cover an area of 3km by 3km (i.e., 128 by 24m on the side).

Visualizations for Test Area Brazeau

Figures 4 and 5 show two geometrically ortho-rectified radar images of an area east of the Brazeau range in Alberta, Canada. Rectification was accomplished with a height model obtained from a stereo-radargrammetric process. The area has a relief variation of 478m and fairly uniform surface cover.

The two rectified radar images and the stereo derived height model (Figure 6) are input to the shape-from-shading process. The resulting height model is presented in Figure 7. The visualization of the Digital Elevation Models (DEMs) is based on an "illumination" from the west, in analogy to the radar illumination. Visual inspection reveals the improved detail in the shape-from-shading DEM when compared to the stereo case.

Figures 8 and 9 illustrate the difference between the two DEMs with the use of contour lines, superimposed over one of the rectified radar images. The refinement of detail in the height model as a result of the shape-from-shading process is evident. Superimposition with the image permits the judgment to be made that the detail is consistent with the radar image.

Analysis of Height Accuracy

The study area of Figures 4 to 9 is also covered by a DEM derived by classical photogrammetry using aerial photography

FIG. 4. Ortho-rectified input radar image (Area: East of Brazeau Range, Canada. Pixel size = 24 m; Size of area - 128 by 128 pixels or 3km by 3km). Radar image produced by Intera Technologies Ltd., Calgary, Canada, using the STAR-2, X-band SAR with 6-m resolution at seven looks. Look angle off-nadir approx. 71°.

FIG. 5. Ortho-rectified input radar image. Same area as Figure 4, but imaged with a look angle off-nadir of 58°.

FIG. 6. Illuminated radar stereo derived height model using the images in Figures 4 and 5 as input, together with Global Positioning System navigation data. Illumination angle is 58° to obtain similarity to SAR images. Terrian height differences are about 478 m. RMS height errors were determined by comparison to a map and amount to ± 25m. Note that this error causes a neglect of morphological detail. Spacing of the stereo measurements was about 250m.

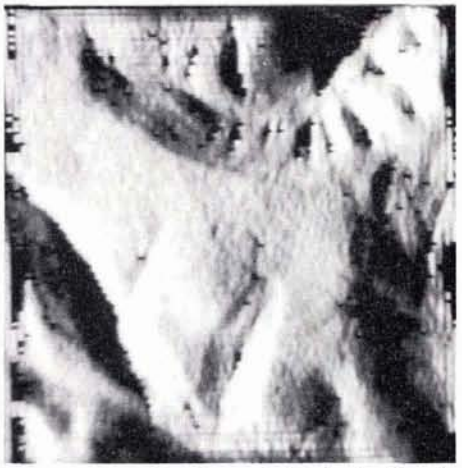

FIG. 7. Illuminated height model derived with radar shape-from-shading using as input the images in Figures 4, 5, and 6. Note the increase in detail when compared to the stereo-result (Figure 6) and the removal of stereo-induced artifacts. Striping along the area's edges is an artifact induced by "ringing" in the Fourier-Transforms.

FIG. 9. Radar shape-from-shading derived contour lines are here superimposed over the radar image of Figure 4. Comparison with Figure 8 reveals an improved modeling of geomorphological structure. Contour interval is also 40m. Ringing effects along the edge of the area are artifacts.

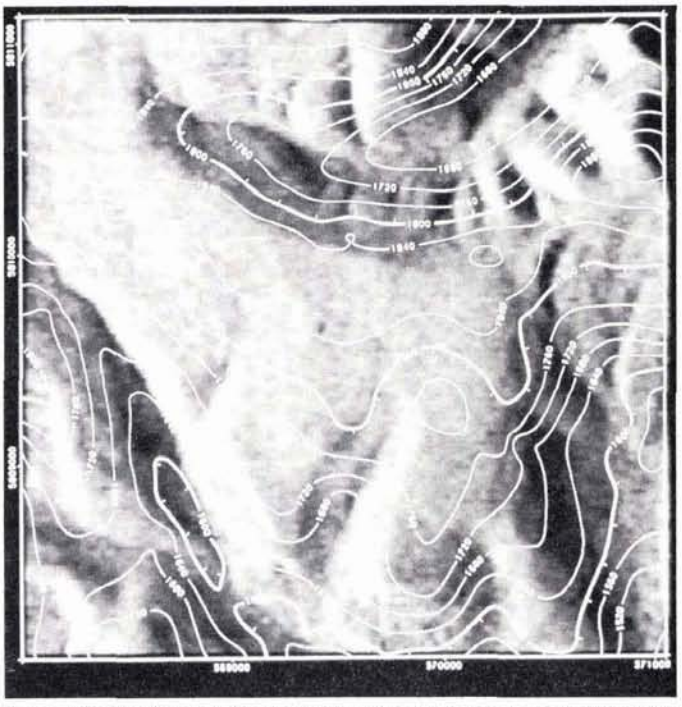

FIG. 8. Radar stereo derived contour lines are superimposed over the rectified radar image in Figure 4. Contour line interval is 40m; contours are computed from the Digital Elevation Model. Note the fact that the contour lines fail to model geomorphological structure, e.g., in the upper right corner of the 3km by 3km area.

FIG. 10. Photogrammetric height model with the heights linearly mapped into brightness values. Source: Aerial wide-angle photography at a scale of 1:50,000, permitting an accuracy in height of the Digital Elevation Model of about ± 1m. Area is 3km by 3km, covering a segment of Brazeau for comparison with the radar images in Figures 4 and 5.

at a scale of 1:50,000. The measurement of a surface point is expected to be accurate to within ±1m. Therefore, the photogrammetric stereo model can be considered as "ground truth," and is presented in Figure 10. Figures 11 and 12 show the radar stereo and shape-from-shading derived height models. The three DEMs can be compared (Table 1). As expected, the shape-from-shading technique has not improved the absolute measure of accuracy in a significant manner (an improvement of only 3m over radar stereo alone). It is the refined detail that is contributed by shape-from-shading.

ANALYSIS OF HEIGHT PROFILES

In order to further evaluate the height accuracy, profiles of the three height models are plotted and compared in Figure 13. The plot is of a profile through the radar stereo derived and

FIG. 11. Radar stereo height model with the heights linearly mapped into brightness values permits comparison with photogrammetric data set of Figure 10 (see also Figure 6).

FIG. 12. Radar shape-from-shading height model with the height linearly mapped into brightness values for comparison with the photogrammetric data set in Figure 10. Again, note the improved similarlity with the photogrammetric data, when compared to the less accurate data of Figure 1 from radar stereo.

TABLE 1. ROOT MEAN SQUARE DIFFERENCE OF DIGITAL ELEVATION MODELS SUBTRACTING HEIGHT VALUE AT IDENTICAL PLANE POSITIONS, COMPUTED OVER 11,664 POINTS LOCATED IN THE 3-KM BY 3-KM TEST AREAS OF FIGURES 4 TO 12

Height Models Compared	Standard Deviation of Height Error
Photogrammetric Model vs. Radar Stereo Model	25 m
Photogrammetric Model vs. Radar Shape-from-Shading	22m

optical stereo derived height models, while Figure 14 shows height profiles through the radar shape-from-shading derived and optical stereo derived height models. The oscillations at the edges of the shape-from-shading height model are a result of

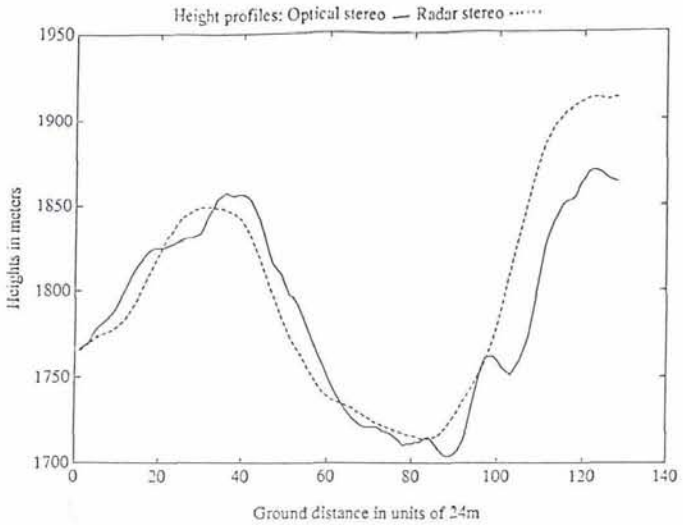

FIG. 13. Comparison of height profile through radar stereo and photogrammetric height models. Note that the radar stereo data deviates on the right edge in a systematic manner. Elevation points were measured every 100m.

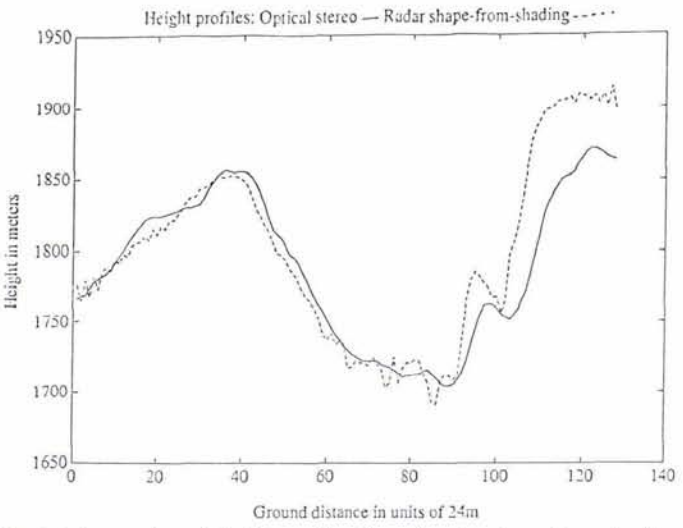

FIG. 14. Comparison of height profiles through radar shape-from-shading and photogrammetric height models. The systematic deviation on the right edge is the result of the radar stereo inaccuracy. The shape-from-shading values are sampled every 24m, the photogrammetric profile has a value only every 100m.

ringing and could possibly be eliminated as described by Lagendijk *et al.* (1988).

As seen from these plots, shape-from-shading has improved the results obtained using radar stereo alone by adding additional detail. Shape-from-shading has also corrected some of the errors present in the radar stereo height model. For example, consider the region between 20 pixels and 60 pixels in Figure 13 and notice the relative shift between the two models. Notice that this shift has been corrected by radar shape-from-shading as shown in Figure 14. Consider, however, the region between 90 and 120 pixels. In this region the relative shift between the radar stereo derived height model and the photogrammetric model was not corrected. The reason for such selective correction by the shape-from-shading algorithm has not been established and is under study. It is anticipated that such relative shifts can be

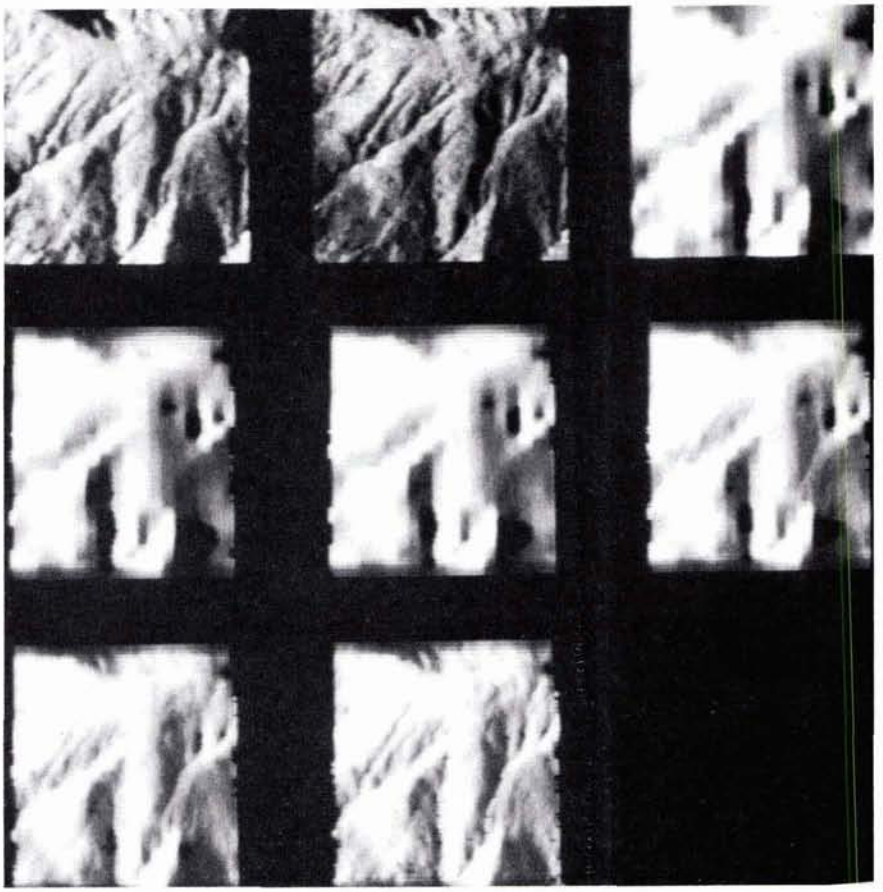

FIG. 15. Sequence of images to illustrate iterative nature of the shape-from-shading alogorithm. (Top row, L-R: Input image 1, input image 2, illuminated radar stereo height model used as input. The remaining images are illuminated height models produced by shape-from-shading at 5, 10, 15, 20, and 25 iterations.)

corrected by iteratively re-rectifying the images input into shape-from-shading. A re-rectification technique has been formulated and is currently being implemented.

Because the photogrammetric height model was created at a 100-m grid and interpolated to 24m (to compare to the radar models), some of the detail present in the shape-from-shading derived height model is not reflected in the photogrammetric height model. This is especially true in the regions between 70 and 90 pixels in Figure 14. Nevertheless, the current photogrammetric model serves as accurate ground truth for all analyses except those involving slopes.

ITERATIONS

A sequence of images illustrates the iterative nature of the shape-from-shading process for a tropical forested area. Ground truth is not available for this area. Therefore, only a visual analysis of the results is feasible as shown in Figure 15. Two rectified radar images and the radar stereo derived DEM are the input to shape-from-shading. The effect of iteractions is illustrated at the completion of 5, 10, 15, 20, and 25 iterations. One notes the gradual addition of detail into the height model as the number of iterations increases.

IMAGES OF GLACIERS

Figure 16 represents a test case using two radar images of glaciers on Baffin Island, Canada. Again, no ground truth exists for the area. The stereo-process is only marginally applicable because the glacier ice provides a poor surface definition. The stereo-DEM presents some outright errors where artifacts are being generated. The shape-from-shading process seems to correct these artifacts and provides a DEM that is consistent with the image gray values.

IMAGES WITH SLOPE EFFECTS REDUCED

One benefit of a radar-derived DEM is its use in the interpretation of image gray values. A direction of future study will provide the terrain analyst a set of processed radar images where slope-induced variations in image gray values are removed, and variations in gray values can be interpreted as an effect of surface properties.

Figures 17 and 18 are examples of images where slope effects are removed. Creation of such images has been described by Domik *et al.* (1986, 1987) and Thomas *et al.* (1989c). Note that shape-from-shading leaves less detail in these images than does the use of a stereo-DEM.

It is anticipated that the interpretation of multiple radar images will benefit from an ability to interactively define backscatter curves, to use these for shape-from-shading, and to analyze the results in the form of rectified, slope-effect-reduced images.

CONCLUSIONS AND RECOMMENDATIONS

Results were obtained so far with a reflectance map that follows the cosine law. Inspite of this simplifying assumption, the shape-from-shading algorithm provided improvements to the

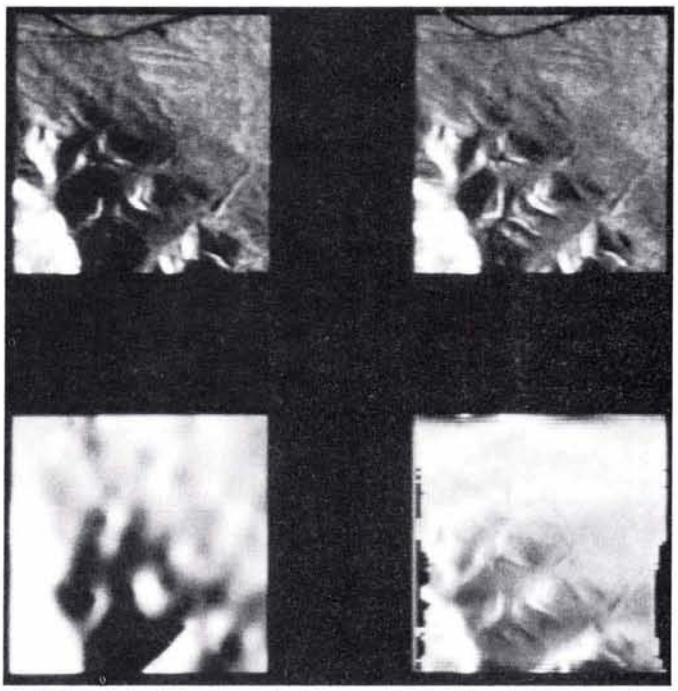

FIG. 16. Test of shape-from-shading over Baffin Island. (Top row - input radar images. Bottom row - illuminated radar stereo height model (left) and illuminated radar shape-from-shading model (right).) Area is 3km by 3km, imaged with STAR-2 of Intera Technologies Ltd., Calgary, Canada, at x-band, 6-m resolution, seven looks. Incidence angles of the input images are 51° and 70°.

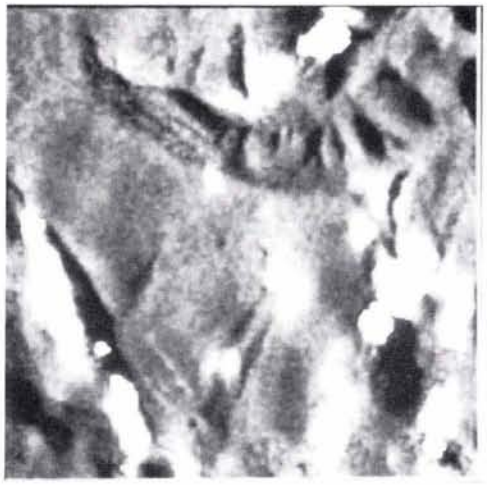

FIG. 17. This is a "secondary" radar image of the 3km by 3km area shown in Figure 4. The gray values in the input image are modified to remove the effect of terrain slope. Where white areas exist, we find a modification that is grossly in error. The terrain slope used for the correction is obtained from the radar stereo model (see Figure 6). The technique used for the creation of such "slope-effect-reduced" radar images was described by Domik *et al.* (1986). If the terrain slopes were error free, and the surface cover uniform, then this "slope-effect-reduced" image would be monotonously gray.

FIG. 18. This represents the same result as Figure 17, but employing the terrain slopes from radar shape-from-shading. Note that there is far less structure in this image than was found in Figure 17, leading one to conclude that the terrain slopes were more accurate than those used in Figure 17. The remaining areas of white exist where terrain slopes seem to be in error.

stereo-based height model. Improvements were illustrated qualitatively with various aircraft radar image sets. Quantitative assessment of improvements by shape-from-shading are hampered by a lack of data sets with ground truth.

A single radar data set was available for which also a photogrammetric digital elevation model (DEM) was measured. Height accuracies were 22m, using stereo and shape-from-shading, while it was 25m using radar stereo alone. While the improvement in absolute accuracy is modest, it appears dramatic in morphological detail.

We anticipate using more accurate models of the reflectance maps in combination with images acquired by radiometrically calibrated radar systems in future studies. One approach involves using a fully polarized multi-frequency radar to infer additional properties of the surface, and to more accurately model the reflectance map. Such additional information could be used to iteratively correct the estimate of the reflectance map. An iterative approach has been mathematically formulated and has produced significant height accuracy improvements when applied to one-dimensional data sets as presented by Thomas *et al.* (1989a). The implementation of the two-dimensional version of this algorithm is under study.

Numerous other improvements include the iterative re-rectification of the input radar images based on the latest height model estimates and the change of the software to employ additional constraints as the shape-from-shading iteractions occur.

The Magellan mission to map planet Venus is a major driver for the development of this technique. The polar area of Venus will be covered by many images and will lend itself to an analysis utilizing this technology. The opportunity exists to assess the results in a comparison with interferometrically measured elevations. The lower latitudes of the planet will not offer an opportunity for interferometry. Shape-from-shading will be the only applicable technique in this case, at least for the nominal mission. If an extended mission results in additional image coverages, one may be able to improve the accuracy of he surface reconstruction by adding stereo observations and independent shading data.

ACKNOWLEDGMENTS

The work reported here was funded by NASA and JPL for the Magellan radargrammetric effort (Contract #957955 and

Contract #958594). The images used in the study were provided by Intera Technologies Ltd. The authors would like to thank D. Meyer for his interest in this effort and the numerous stimulating discussions. We would also like to thank S. Fuchs for her help in preparing this report.

REFERENCES

Baltes, H. P. (ed.), 1980. *Inverse Scattering Problems in Optics*, Springer.

Domik, G., F. Leberl, and J. Cimini. 1986. Multiple Incidence Angle SIR-B Experiment over Argentina-Generation of Secondary Image Products, *IEEE Trans. Geoscience and Remote Sensing*, Vol. GE-24, pp. 492–497.

Domik, G., and F. Leberl, 1987. Image Based SAR Product Simulation for Analysis, *Proc. 53rd Ann. Conv.*, American Society of Photogrammetry and Remote Sensing, Baltimore, Maryland, pp. 249–263.

Frankot, R., and R. Chellappa, 1987a. Application of a Shape-from-Shading Technique to Synthetic Aperture Radar, *Proc. Int'l Geoscience and Remote Sensing Symposium*, Ann Arbor, Michigan.

———, 1987b. A Method for Enforcing Integrability in Shape-from-Shading Algorithms, *Proceedings of Int. Conf. on Computer Vision*, London, England.

Guindon, B., 1989, Development of a Shape from Shading Technique for the Extraction of Topographic Models from Individual Spaceborne SAR Images, *Proc of IGARSS 1989*, Vol. 2, pp. 597–602, Vancouver, Canada.

Horn, B., and M. Brooks, 1986. The Variational Approach to Shape from Shading, *Computer Vision, Graphics and Image Processing*, Vol. 33.

———, 1989. *Shape from Shading*, The MIT Press, Cambridge, Massachusetts, London, England.

Kaupp, V., H. MacDonald, and W. Waite, 1981. *Image Radar: Analysis of Propagation Distortions*, Arkansas Remote Sensing Laboratory Technical Report, ARSL TR 81-1, Univ. Arkansas, Fayetteville.

Kirk, R. L., 1987. *A Fast Finite-Element Algorithm for Two-Dimensional Photoclinometry*, Dissertation, California Institute of Technology.

Leberl, F., 1976. *Accuracy Aspects of Stereo Side-Looking Radar*, JPL Publication.

Lagendijk, R. L., J. Beimond, and D. Bockee, 1988. Regularized Iterative Image Restoration Ringing Reduction, *IEEE Trans. on Acoustics, Speech, and Signal Processing*, Vol. 36, No. 12.

Marion, J. B. 1965. *Classical Dynamics of Particles and Systems*, Acad. Press.

Mercer, J. B., P. Button, M. Millot, K. Karspeck, and F. Leberl, 1989. Topographic Mapping from GPS-Supplemented Airborne Radar, *Proc. of IGARSS 1989*, Vol. 4, pp. 2466–2467, Vancouver, Canada.

Ramapriyan, H. K., J. P. Strong, Y. Hung, and C. W. Murray, 1986. Automated Matching of SIR-B Images for Elevation Mapping, IEEE Trans. *Geoscience and Remote Sensing*, Vol. GE-24 No. 4, pp. 462–472.

Schey, H. M., 1973. *Div, Grad, Curl, and All That*, W. W. Norton and Co. Inc., New York.

Shao, M., T. Simchomy, and R. Chellappa, 1988. New Algorithms for Reconstruction of a 3-D Depth Map Frame One or More Images, *Proc. of Computer Vision and Pattern Recognition*, Ann Arbor, Michigan.

Thomas, J., V. Kaupp, W. Waite, and H. MacDonald, 1987. Optimum Considerations for Radar Stereo, *Proc. IGARSS 1987*, Ann Arbor, Michigan.

Thomas, J., D. Meyer, W. Kober, and F. Leberl, 1989a. *SAR Polarimetry and Multiple Image Shape-From-Shading for Terrain Reconstruction*, VEXCEL Corp. Phase I SBIR Technical Report.

Thomas J., W. Kober, and F. Leberl, 1989b. Multiple-Image SAR Shape-from-Shading, *Proc. of IGARSS 1989*, Vol. 2, pp. 592–596, Vancouver, Canada.

———, 1989c. *Automated Stereo Correlation*, VEXCEL report prepared under Contract #(JTX-C-0193-00) for Mitsubishi International Corporation.

Wildey, R., 1986a. Radarclinometry for the Venus Radar Mapper, *Photogrammetric Engineering & Remote Sensing*, Vol. 52, No. 1, pp. 41–50.

———, 1986b. Radarclinometry, *Earth, Moon, and Planets*, Vol. 36, pp. 217–267.

———, 1987. The Line Integral Approach to Radarclinometry, *Earth, Moon, and Planets*, Vol. 38, pp. 59–95.

———, 1988a. The Surface Integral Approach to Radarclinometry, *Earth, Moon, and Planets*, Vol. 41, pp. 141–153.

———, 1988b. Radarclinometry: Bootstrapping the Radar Reflectance Function from the Image Pixel-Signal Frequency Distribution and an Altimetry Profile, *Earth, Moon and Planets*, Vol. 41, pp. 223–240.

(Received 19 March 1990; accepted 16 April 1990)